International Journal of Structural Stability and Dynamics

Investigation on aerodynamic fluid-structure coupling vibration of 160 km/h EMU tail in single-track tunnels

--Manuscript Draft--

Manuscript Number:	IJSSD-D-23-00733
Full Title:	Investigation on aerodynamic fluid-structure coupling vibration of 160 km/h EMU tail in single-track tunnels
Article Type:	Research Paper
Section/Category:	
Keywords:	160 km/h EMU; tail swaying; ride comfort; fluid-structure coupling; vortex-induced vibration
Corresponding Author:	Yuan Yao Southwest Jiaotong University State Key Laboratory of Traction Power CHINA
Corresponding Author Secondary Information:	
Corresponding Author's Institution:	Southwest Jiaotong University State Key Laboratory of Traction Power
Corresponding Author's Secondary Institution:	
First Author:	Yadong Song
First Author Secondary Information:	
Order of Authors:	Yadong Song
	Ting Qing
	Yuan Yao
	Fengyu Dai
Order of Authors Secondary Information:	
Abstract:	Recently, the phenomenon about tail sustained swaying of the 160 km/h EMU in single-track tunnels has gained much attention, especially for the rear powered vehicle. This phenomenon is investigated from the perspective of aerodynamic fluid-structure coupling vibration in this study. The aerodynamics simulation model of the train in tunnels and the multi-body dynamics model of the rear powered vehicle were respectively established through the software of XFlow and Simpack, and then the fluid-structure coupling vibration was simulated by using real-time data dynamic exchange between the two models. Moreover, the carbody's vibration acceleration and the aerodynamic loads acting on the carbody under various wheel-rail contact geometrical conditions were discussed. Finally, the train tail swaying in field was tested, and the dominant frequencies were analyzed. The results show that the periodic aerodynamic loads and the frequency locking effect caused by the coupled vibration are the main factors for the ride comfort deterioration. The violent vibration caused by fluid-structure coupling is named vortex-induced vibration (VIV) in some industries, such as bridge, submarine pipeline, etc. For the vehicle in this work, with the decrease of equivalent conicity in wheel-rail contact, the amplitude of carbody swaying increases owing to the carbody hunting, which enhances the fluid-structure coupling vibration, and further deteriorates the ride comfort. The swaying of the carbody is dominated by the vehicle hunting frequency, and the improvement of vehicle lateral stability can weaken this phenomenon.
Suggested Reviewers:	Yongqiang Liu Shijiazhuang Tiedao University LIUYQ@STDU.EDU.CN
	Liang Ling

	Southwest Jiaotong University State Key Laboratory of Traction Power liangling@swjtu.edu.cn
	Jiwang Zhang Southwest Jiaotong University State Key Laboratory of Traction Power zhangjiwang@swjtu.cn
	Gongquan Tao Southwest Jiaotong University State Key Laboratory of Traction Power taogongquan@swjtu.edu.cn

Investigation on aerodynamic fluid-structure coupling vibration of 160 km/h EMU tail in single-track tunnels

Yadong SONG[1], Ting QIN[1], Yuan YAO[1✉], Fengyu DAI[2]

[1]*State Key Laboratory of Rail Transit Vehicle System, Southwest Jiaotong University, Chengdu 610031, China*;

[2]*Dassault Systemes INFORMATION Technology Co., Ltd., Shanghai 200120, China*.

Abstract

Recently, the phenomenon about tail sustained swaying of the 160 km/h EMU in single-track tunnels has gained much attention, especially for the rear powered vehicle. This phenomenon is investigated from the perspective of aerodynamic fluid-structure coupling vibration in this study. The aerodynamics simulation model of the train in tunnels and the multi-body dynamics model of the rear powered vehicle were respectively established through the software of XFlow and Simpack, and then the fluid-structure coupling vibration was simulated by using real-time data dynamic exchange between the two models. Moreover, the carbody's vibration acceleration and the aerodynamic loads acting on the carbody under various wheel-rail contact geometrical conditions were discussed. Finally, the train tail swaying in field was tested, and the dominant frequencies were analyzed. The results show that the periodic aerodynamic loads and the frequency locking effect caused by the coupled vibration are the main factors for the ride comfort deterioration. The violent vibration caused by fluid-structure coupling is named vortex-induced vibration (VIV) in some industries, such as bridge, submarine pipeline, etc. For the vehicle in this work, with the decrease of equivalent conicity in wheel-rail contact, the amplitude of carbody swaying increases owing to the carbody hunting, which enhances the fluid-structure coupling vibration, and further deteriorates the ride comfort. The swaying of the carbody is dominated by the vehicle hunting frequency, and the improvement of vehicle lateral stability can weaken this phenomenon.

Keywords: 160 km/h EMU; tail swaying; ride comfort; fluid-structure coupling; vortex-induced vibration

1 Introduction

Since the operation of the Power Centralized EMU (Electric Multiple Unit) with a speed of 160 km/h in 2019, the EMUs have appeared different lateral dynamics problems. Including the phenomenon of vehicle hunting instability [1–3], the difference in lateral ride comfort between the front and rear ends of the same carbody [4], even the serious ride comfort deterioration of the tail vehicle in single-track tunnels [5]. In the single-track tunnel, whether the long-marshalling or short-marshalling trains, the sustained swaying of the rear powered vehicle (i.e. locomotive) is unbearable for the driver, while the lateral ride comfort of the other non-powered vehicles and the front powered vehicle is excellent. In this regard, this phenomenon is suspected to be caused by the aerodynamic effect, and the realization promotes this works.

The theory of vortex-induced vibration (VIV) has been extensively studied in slender structures such as bridge, submarine pipeline, etc. The VIV is one of the typical flow-induced vibrations, and the phenomenon happens when the vortex shedding frequency becomes close to one of the natural frequencies of the structure [6]. Concurrently, the frequency of aerodynamic force is “locked” to the natural frequency [7]. The train has the significant characteristics of large slenderness ratio in terms of fluid mechanics, which is quite different from other land vehicles. Meanwhile, due to the interaction between the underside flow and the ground, the air flow around the train is still different from that of the aircraft. As the geometrical characteristics and running speed of the train, the generated flow field is essentially a three-dimensional turbulent flow field [8]. Hemida and Krajnovic [9] found that the tail vortex structure of the train is similar to the Karman vortex street, and the carbody lateral vibration will be aggravated if the vortex shedding frequency is close to the lateral vibration frequency of the carbody.

Up to now, there exists three main methods used to study the aerodynamic characteristics of the trains, including physical model tests, numerical simulation and computational fluid dynamics (CFD) [10]. The physical model tests mainly include field and wind tunnel tests. These tests are expensive and complicated to set up, and are also affected by external conditions. The numerical simulation is simple and easy to control, but the result is essentially an approximate solution, and is often different from the actual operating conditions, so it is more suitable for the theoretical research

[11]. Computational resources are the main limitation to CFD simulation, and the application of ground vehicles requires numerous calculations. Nowadays, with the rapid development of computer resources, the application of CFD in the field of vehicle aerodynamics has increased significantly [12].

The aerodynamic effect in tunnels is significant with the increase of train speed, which leads to issues such as aerodynamic noise and ride comfort deterioration caused by vehicle swaying. Therefore, it is essential to research the aerodynamic performance of the train operating in tunnels. Choi et al. [13] studied the influence of train speed, nose length and blockage on the aerodynamic drag of the train in subway tunnels through CFD simulation. Niu et al. [14] studied the influence of Reynolds number on the train surface pressure in the tunnel through scaled models, and explained the relationship between the Reynolds and pressure amplitude. Du et al. [15] investigated the influence of vehicle number on the aerodynamic pressures of tunnel lining and micropressure waves at tunnel portals by three-dimensional numerical simulation.

The phenomenon of train swaying in tunnels was first observed in the Shinkansen of Japan in 1993. Moreover, the lateral swaying of the carbody was the most obvious, and the swaying of the marshalling train gradually increased from the head vehicle to the tail vehicle [16]. Many studies have been done to research the phenomenon of train swaying in tunnels. Takai [17] first confirmed that the track irregularity has little effect on the swaying of the train in tunnels, and the aerodynamic force is the main factor. Suzuki [18,19] has carried out large numbers of experiments and numerical analysis, which shows that the tail vortex eddying is the reason for the ride comfort deterioration when the train is running in the tunnel. Diedrichs et al. [20,21] used the large eddy simulation (LES) method to analyze the tail carbody's vibration of the German ICE2 high-speed train and the Japanese S300 Shinkansen train in the tunnel, and found that the tail carbody's vibration is related to the shape of the train tail and the mass of the carbody. Tanifuji and Kikko [22,23] established an aerodynamic force model based on the measured pressure data of the test carbody, and analyzed the ride comfort of the train running in the tunnel.

To the best knowledge of the authors, almost all existing researches applied the calculated aerodynamic loads to the vehicle dynamics model as an external excitation, whereas little attention is paid to the fluid-structure coupled vibration of the vehicle. Unfortunately, the effect of VIV on the dynamic performance of the train system has been rarely investigated. In this paper, the simulation for fluid-structure coupling vibration of the train was carried out, based on the vehicle multi-body system dynamics model and the aerodynamics model of the 160 km/h EMU running in a single-track tunnel. Furthermore, the carbody's vibration acceleration and the aerodynamic loads acting on the carbody under various wheel-rail contact geometrical conditions were discussed. Finally, the simulation results are compared and verified through the on-track test, and the relevant conclusions are summarized.

2 Dynamics modeling

2.1 Train-tunnel aerodynamics model

The aerodynamics simulation is performed by the commercial CFD software of SIMULIA XFlow 2021x. It uses a proprietary fully Lagrangian particle-based kinetic approach, which is based on the lattice Boltzmann method (LBM) [24–27]. Compared with the traditional grid method simulation, the main advantage of XFlow based on particle method is that it can easily simulate the conditions of moving components and fluid-structure interaction, and its adaptive wake refinement function can dynamically track the wake during flow development [28].

The Large Eddy Simulation (LES) is used for turbulence modeling in XFlow, and the LES model is the Wall Adapting Local Eddy (WALE) viscosity model, which provides a consistent local eddy-viscosity and near wall behavior [28]. The LES turbulence models are not widely employed for a long time, since the computation cost is relatively high compared to RANS models with the Navier-Stokes solvers. The LBM scheme allows the use of LES turbulence model at low computational cost. As a relatively advanced research method, the LES turbulence models are good at transient simulation of high turbulence and separated flow, while the RANS models are mostly limited to steady-state analysis. The LES model has been effectively applied to simulate the aerodynamics of a full-scale train in recent years [9,29–31].

The aerodynamics model of the Power Centralized EMU in the single-track tunnel operation used for the CFD simulation is shown in Figure 1(a,b,c). Considering computational resources and the accuracy of aerodynamics calculation for the long train set, a suitable full-scaled model of the train with 6 vehicles and a 400 m long tunnel is established for the research. The vehicle consists of coaches and simplified bogies but without the pantograph and accessory structures. The length of the tail vehicles is 4.4*H*, the length of the middle vehicles is 6.38*H*, and the width of each vehicle is 0.83*H*. The height *H* is 4.0 m at full scale, and *H* is also defined as the characteristic length, which is the height from the top surface of the rail to the roof of the train [32]. In addition, the height of the single-track tunnel is 6.55 m, and its width is 4.88 m according to the standard of GB 146-2 [33]. Referring to the literatures [32,34], the height from the lower surface of the wheelset to the ground is set to 0.05*H*, and the length of intercarriage gap is set to 0.1*H*.

The computational domain and the boundary conditions are shown in Figure 1(d). The total length of the computational domain is 100*H*, which is large enough for the development of flow field. For the single-track tunnel, the inlet and outlet boundary conditions are set to velocity inlet and pressure outlet, respectively. The inlet velocity *U* is the running speed of the train along the x-axis, and the outlet pressure is set to 0. The train is positioned at the 20*H* downstream of the inlet boundary, and the wake field extends for 45*H* in the x-direction, which can effectively reduce the interference of the outlet boundary on the train wake according to the standard of EN 14067-6 [35]. In addition, the boundary conditions of the inner wall around the tunnel and the train surface are set as the wall model of non-equilibrium enhanced wall-function, which is strongly recommended for aerodynamic applications in XFlow, because it takes into account the pressure gradients to predict the boundary layer separation [28]. In this simulation, the Reynolds number calculated through the following formula is 8.09×10^6.

$$Re = \rho UH / \mu. \tag{1}$$

where the air density ρ is 1.007 kg/m³, and the air viscosity coefficient μ is 17.9×10^{-6} Pa·s, at the atmospheric pressure of 79.158 kPa in Yunnan, China with the altitude of 2,000 m. Moreover, the velocity *U* of the incoming flow is 36 m/s (130 km/h), and the characteristic length *H* is 4.0 m.

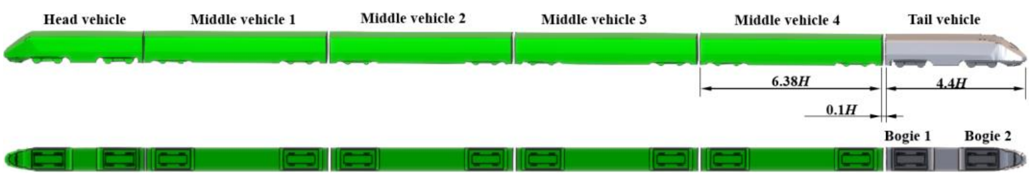

(a)

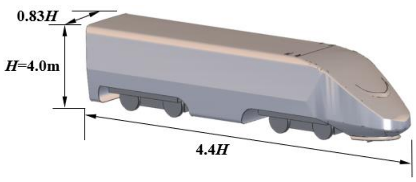

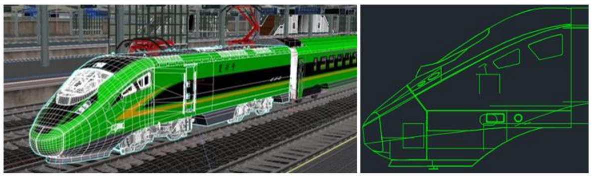

(b) (c)

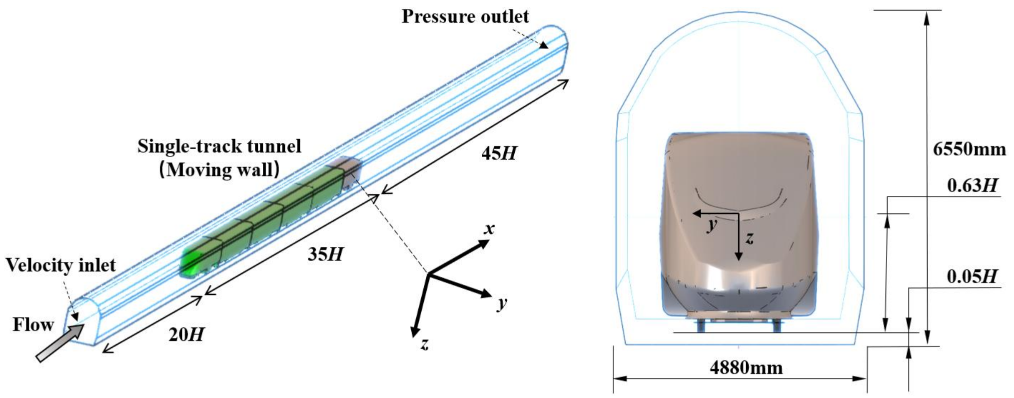

(d)

Figure 1. Aerodynamics model of full-scale train tunnel: (a) train model; (b) tail vehicle shape; (c) actual train head shape; (d) computational domain and boundary conditions.

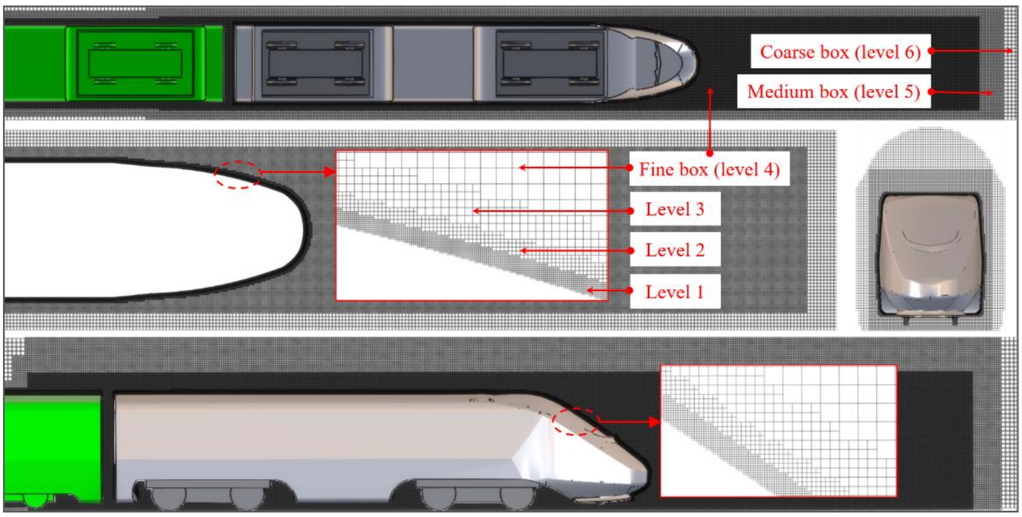

Figure 2. Computational particle in single-track tunnel.

In this work, the computational particle of CFD is the octree lattice structure based on the input geometries, and the octree lattice structure generated by XFlow is D3Q27 organized [28]. Considering the structure of the train and in order to better simulate the vortex structures of the train wake, the dynamic wake refinement is applied and three refinement boxes are used, as shown in Figure 2. Furthermore, three kinds of particle densities are adopted to verify the grid independently, and the details of particle settings are shown in Table 1. The results of grid-independence study are shown in Figure 3. It can be seen that with the increase of particle density, the aerodynamic lateral force F_y of the tail vehicle tends to be stable, which is similar to the results in reference [18]. Therefore, six levels of octree structure are generated, of which the particle resolution in the far field (level 6) is 0.064H, and the resolution of the refined particle (level 1) near the tail carbody surface and in the wake is 0.002H.

Table 1. Calculation case of particle density.

Calculation case of particle density	Refined particle size (level 1) /m	Coarse particle size (level 6) /m	Total number of particles /$\times 10^5$
Case1	0.005H	0.16H	93
Case2	0.003H	0.096H	167
Case3	0.002H	0.064H	238

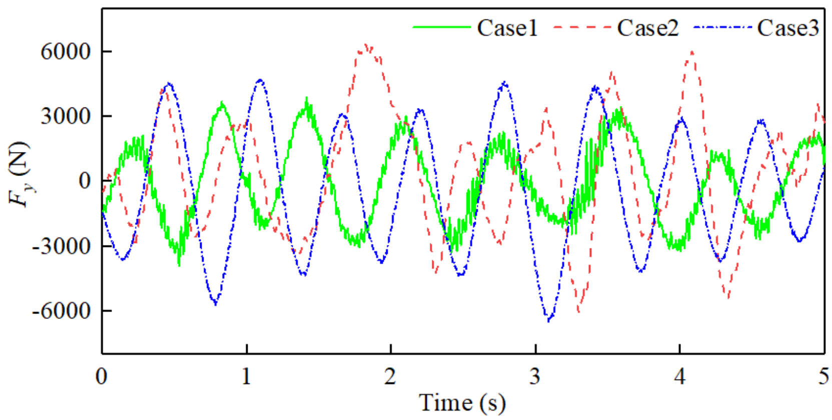

Figure 3. Grid-independence study.

2.2 Vehicle multi-body dynamics model

The rear powered vehicle (B0-B0 locomotive) dynamics model of the Power Centralized EMU is established by the commercial multi-body dynamics software SIMULIA Simpack 2020, as shown in Figure 4. The dynamics model is composed of 25 rigid bodies, including one carbody, two bogie frames, two traction rods, four wheelsets, four motors, four hollow shafts and eight axle box rotating arms, with a total of 90 degrees of freedom (DoF). Among them, the carbody, bogie frame, wheelset and motor have six DoFs of translation and rotation in x/y/z-directions. Each hollow shaft has three DoFs in lateral, rolling, and yaw motions around the wheelset, and every traction rod has two DoFs in yaw and pitch motion relative to the carbody. Nevertheless, each rotating arm only has one DoF in rotational motion relative to the wheel axle. Besides, the track gauge is set to 1435 mm, and the wheel-rail tangential force is calculated by the FASTSIM algorithm [36] in Simpack. Moreover, the high-speed track spectrum [37] is adopted as the track excitation in the following time-domain simulation.

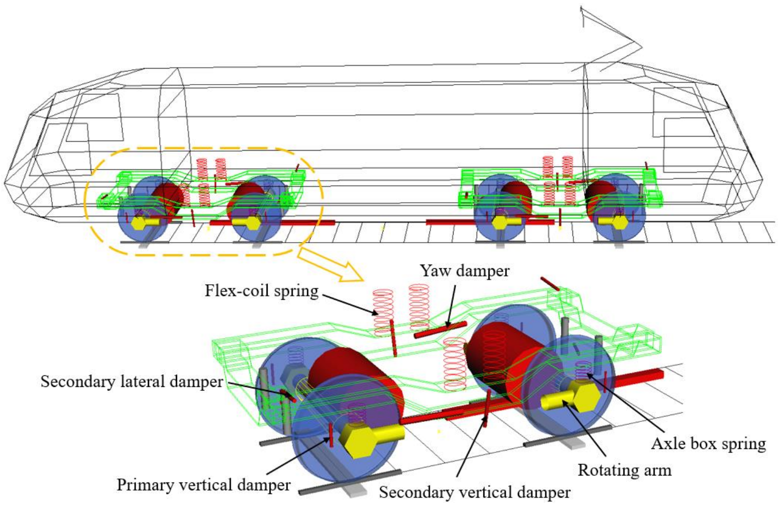

Figure 4. Powered vehicle dynamics model.

Generally, the suspension system of the powered vehicle is composed of primary suspension and secondary suspension. The primary suspension acts between the wheelset and the bogie frame, including rotating arm, axle box spring, and primary vertical dampers. The secondary suspension acts between the bogie frame and the carbody, consisting of the flex-coil spring, secondary lateral damper, secondary vertical damper, yaw damper and secondary lateral stop. In addition, the nonlinear characteristics of dampers and stop elements are considered. The structure and suspension parameters of the powered vehicle are shown in Table 2, and the accuracy of dynamics model has been verified in the previous articles [38,39].

Table 2. Main parameters of the powered vehicle.

Item	Value	Unit
Maximum operation speed	160	km/h
Carbody mass	42.907	t
Bogie frame mass	3.442	t
Wheelset mass	2.434	t

Bogie wheelbase	2.9	m
Distance between bogie centres	9	m
Distance of contact point	1.493	m
Wheel rolling circle diameter	0.625	m
Wheel profile type	JM3/JM3-32	-

2.3 Fluid-structure coupling simulation

Based on the above train aerodynamics model and vehicle dynamics model, the simulation calculation for fluid-structure coupling vibration of the tail powered vehicle in the tunnel was carried out, as shown in Figure 5. According to the *FMU*/*FMI* standard, the fluid-solid coupling vibration is simulated by real-time data dynamic exchange method. The coordinate system origin (0,0,0) is taken at the geometric center of the tail carbody, with a height of 0.63H from the rail surface as shown in Figure 1(d). For the fluid-structure coupling process, the vehicle dynamics model transmits three motion states of the carbody to the train aerodynamics model, including the lateral movement y, roll motion α and yaw motion γ. Then, the train aerodynamics model will transmit the calculated aerodynamic loads including lateral force F_y, roll moment M_x, and yaw moment M_z, to the vehicle dynamics model in real time. In addition, due to the unstable nature of the aerodynamic loads, a unified time step of 0.05 ms and corresponding 800 × 10^3 time-steps are adopted to ensure the full development of the flow in the transient analysis.

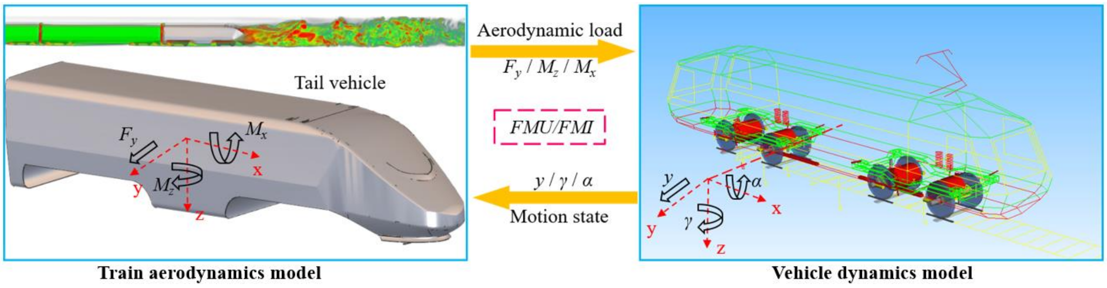

Figure 5. Simulation for fluid-structure coupling vibration of train tail vehicle.

3 Dynamics indexes

3.1 Ride comfort

At present, there are various evaluation methods for running stability and ride comfort of the railway vehicle all over the world, such as VDI 2057, the UK BS 6841, Sperling stationary index, ISO 2631-1, UIC 513, EN 12299, etc., and the last four are relatively commonly used [40]. In this paper, the

Sperling stationary index including lateral and vertical ride comfort is used to evaluate the ride comfort of railway vehicles, and we just analyzed the lateral ride comfort index W_y. The calculation formula of W_y is as follows [41]:

$$W_y = 3.57\left[\frac{A_y^{\;3}}{f}F(f)\right]^{1/10}. \tag{2}$$

where A_y is the lateral vibration acceleration amplitude, f is the corresponding frequency, and $F(f)$ is the frequency correction coefficient. It can be seen that the lateral ride comfort index W_y is obtained through the statistical processing of vibration acceleration, and the measurement location is generally on the carbody floor. In order to study the lateral ride comfort of the rear powered vehicle in this paper, the vibration acceleration of the tail carbody is measured, and the corresponding lateral ride comfort index is obtained. In addition, a smaller value of W_y represents the better lateral ride comfort, and the limit value of the excellent level on lateral ride comfort for locomotive is 2.75.

3.2 Operational safety

In general, the operational safety index of railway vehicle dynamic performance is related to the force on vehicles, such as wheelset lateral force, derailment coefficient, wheel unloading rate and overturning coefficient, and the latter three are suitable for curve and crosswind conditions. Here, the lateral dynamic performance of the train on the straight line is analyzed, so the wheelset lateral force is selected to evaluate the operational safety of the rear powered vehicle. The wheelset lateral force Γ_{WF} is the algebraic sum of the left and right wheel-rail lateral forces on the same wheelset. If the value is too large, it will lead to widening of the gauge or serious deformation of the track. The evaluation of the wheelset lateral force according to the standard of GB/T5599 [40] is as follows:

$$\Gamma_{WF} \le 15 + P_0 / 3. \tag{3}$$

where P_0 is the static axle load in kN, and P_0 of the powered vehicle studied in this paper is about 189 kN, so the limit value of the wheelset lateral force Γ_{WF} is 78 kN.

4 Results and discussion

4.1 Simulation conditions

In this section, based on the actual operating conditions of the train, three calculation conditions are set to simulate the fluid-structure coupling vibration of the rear powered vehicle, corresponding to three different wheel treads, as follows:

Cond 1: JM3_new, with the equivalent conicity of 0.1;

Cond 2: JM3_wear, with the equivalent conicity of 0.4;

Cond 3: JM3-32 thin flange, with the equivalent conicity of 0.04.

The measured wheel profiles of JM3 and the corresponding equivalent conicity of wheel-rail contact are introduced in Section 5 below. In addition, the running speed of the train is set to 130 km/h, and the rail cant is set to 1/40. Furthermore, the vehicle dynamic performances and aerodynamic responses of the rear powered vehicle in the single-track tunnel with different equivalent conicities are analyzed, respectively.

4.2 Vehicle dynamic performances

In order to study the influence of fluid-structure coupling on vehicle dynamic performances, the results of dynamic performances with and without aerodynamic load are shown in Table 3. It can be seen that the aerodynamic effect on the dynamic performances of the rear powered vehicle in the tunnel is mainly reflected on its lateral ride comfort. Without considering the aerodynamic load, as the decrease of equivalent conicity, the lateral ride comfort index W_y of the carbody's rear-end decreases, that is, the carbody swaying is intensified, but it is within the excellent level. When the aerodynamic load is applied, the W_y of the carbody's rear-end exceeds the limit value of 2.75 under Cond 1 and Cond 3, which will lead to the violent vibration of the train tail. However, the aerodynamic load has little effect on the operational safety (wheelset lateral force) of the powered vehicle. Although the wheelset lateral force of the wheelset4 near the train tail is relatively large with aerodynamic load, it is far less than its limit value of 78 kN.

Table 3. Dynamic performances (without/with aerodynamic load)

Calculation condition	Lateral ride comfort W_y		Wheelset lateral force Γ_{WF} (kN)			
	Front-end	Rear-end	Wheelset1	Wheelset2	Wheelset3	Wheelset4
Cond 1	2.08/2.13	2.34/2.90	6.51/7.27	9.19/10.35	5.49/5.87	9.89/11.82
Cond 2	2.03/2.09	2.13/2.67	8.31/8.52	8.50/8.80	7.04/7.28	8.54/9.49
Cond 3	2.00/2.03	2.42/2.95	6.16/6.33	9.70/10.32	4.89/5.10	10.23/11.61

The lateral vibration acceleration of the tail carbody under the Cond 1 with JM3 new wheel profile is analyzed, and the results in time domain and frequency domain are shown in Figure 6. It can be seen from Figure 6(a,c) that the aerodynamic effect in the tunnel mainly aggravates the lateral vibration acceleration of the carbody's rear-end, but has almost no impact on the lateral vibration acceleration of the carbody's front-end. As shown in Figure 6(b,d), the dominated frequency of carbody's lateral vibration is 1.3 Hz without aerodynamic load, which is the vehicle hunting frequency. In addition, under the aerodynamic load, the lateral vibration acceleration response of the carbody is still dominated by the vehicle hunting frequency of 1.3 Hz. The fluid-solid coupling effect will be more obvious at the track section where the lateral vibration of carbody is severe, corresponding to the blue box mark in Figure 6(c).

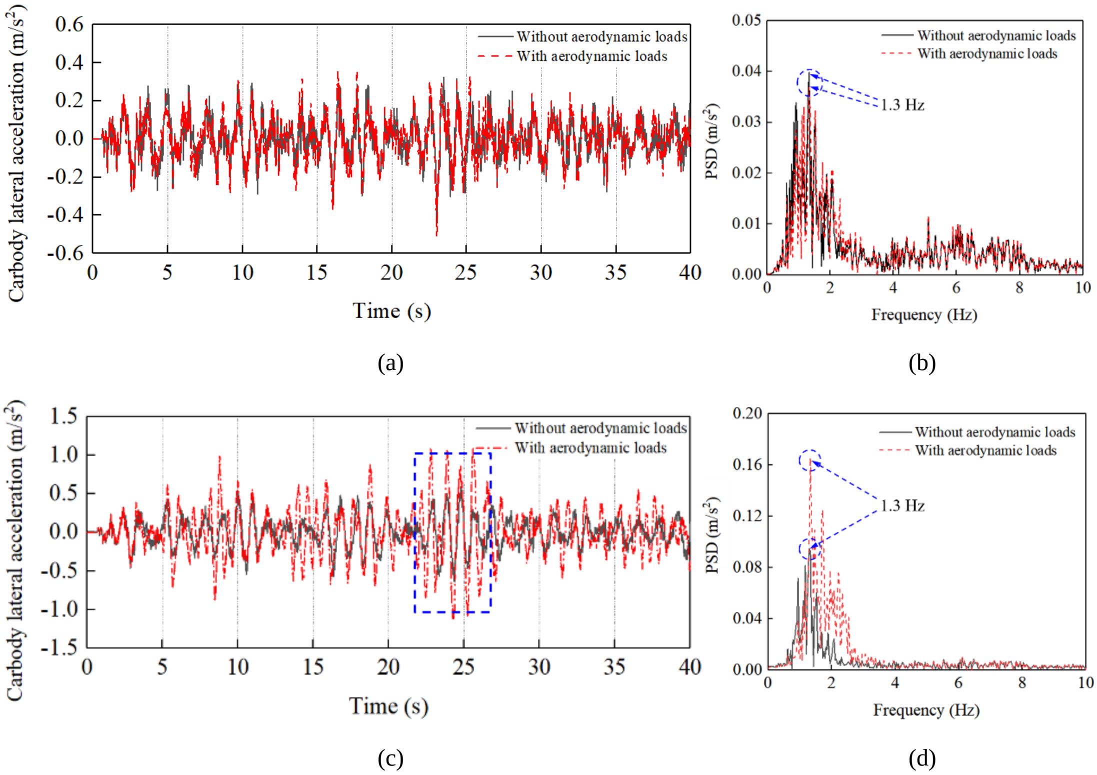

Figure 6. Lateral vibration acceleration of carbody under Cond 3:

(a) time domain in carbody's front-end; (b) frequency domain in carbody's front-end;

(c) time domain in carbody's rear-end; (d) frequency domain in carbody's rear-end.

4.3 Aerodynamic responses

The amplitude of the aerodynamic loads acting on the tail carbody under the three types of wheel-rail contact conditions and carbody fixed condition (calculated separated by aerodynamics model) are shown in Table 4. It can be seen that at the speed of 130 km/h, the amplitude of the aerodynamic lateral force F_y is around 4.5–6.0 kN, the amplitude of the yaw moment M_z is around 35–60 kN·m, and the amplitude of the roll moment M_x is around 1.5–2.5 kN·m.

Table 4. Aerodynamic loads under various wheel-rail equivalent conicities

Calculation condition	Equivalent conicity λ	Amplitude of the aerodynamic force/moment		
		F_y (kN)	M_z (kN·m)	M_x (kN·m)
Cond 1	0.1	5.5	52.8	2.2
Cond 2	0.4	4.8	38.1	1.6
Cond 3	0.04	5.7	56.3	2.0
Carbody fixed	-	6.1	50.5	2.3

Then, the aerodynamic responses of high wheel-rail equivalent conicity Cond 2 and low equivalent conicity Cond 3 are compared and analyzed. The time domain results within 5–35 s and the corresponding frequency domain results are shown in Figure 7. As shown in Figure 7(a,c,e), due to the turbulence of wake vortex in the tunnel, the aerodynamic loads acting on the carbody of the rear powered vehicle is also unstable, which is approximately sinusoidal with time. Meanwhile, with the decrease of equivalent conicity, the carbody swaying is intensified, and the amplitude of the aerodynamic loads acting on the carbody increases, which means that the fluid-structure coupling effect is enhanced. As can be seen from Figure 7(b, d, f), with the increase of carbody swaying, the frequency of the aerodynamic loads acting on the train tail, also known as vortex shedding frequency, changes from 1.7 Hz to the vehicle hunting frequency 1.3 Hz, indicating that the frequency locking of vortex-induced vibration (VIV) phenomenon happens. The fluid-structure coupling effect changes the vortex shedding frequency and causes structural resonance.

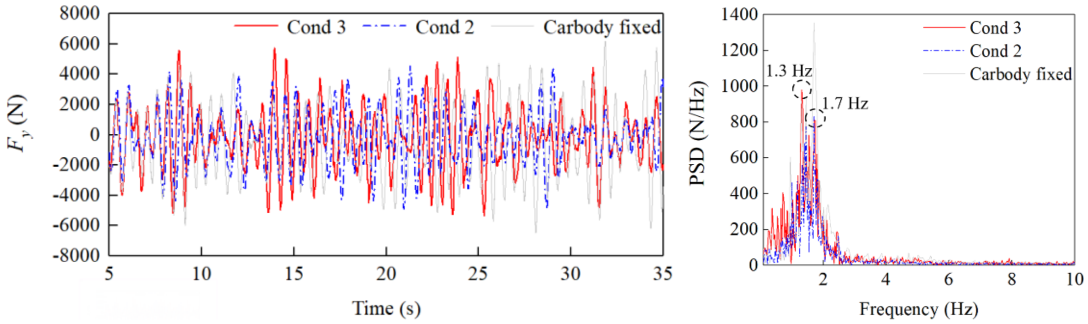

(a) (b)

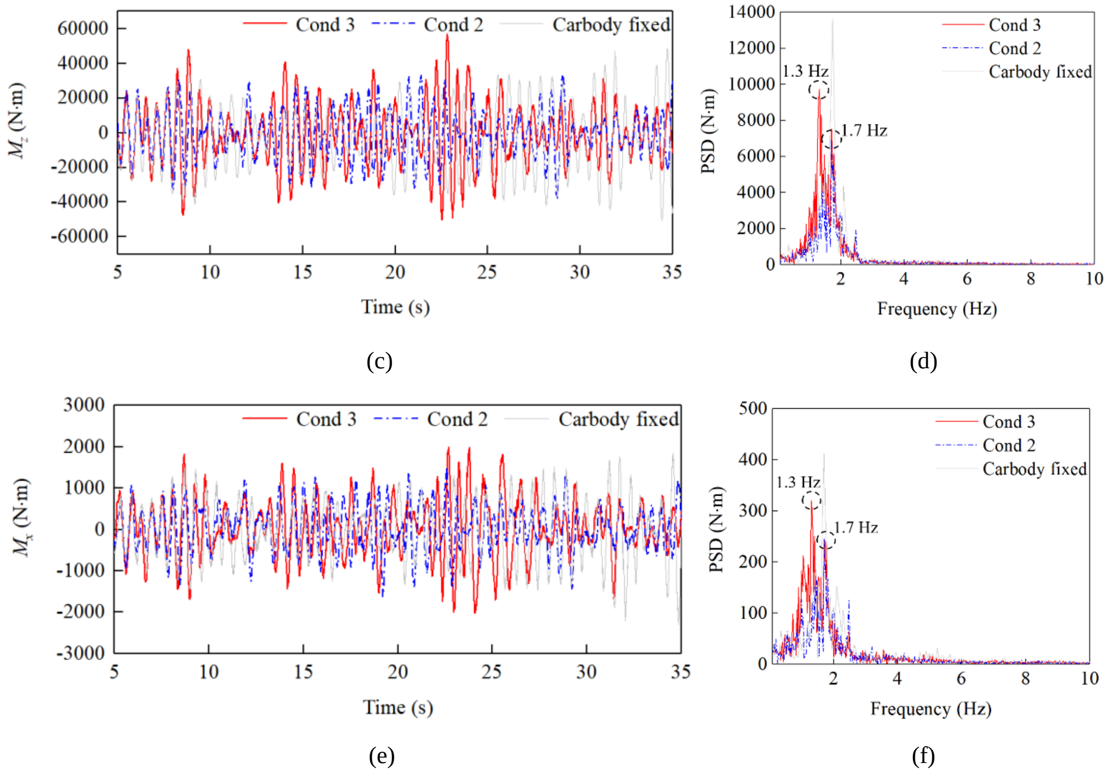

Figure 7. The aerodynamic loads under Cond 3 and Cond 2: (a) time domain in F_y; (b) frequency domain in F_y; (c) time domain in M_z; (d) frequency domain in M_z; (e) time domain in M_x; (f) frequency domain in M_x.

5. On-track tests

According to the responses of the railway attendants and drivers, the overall dynamic performance of the Power Centralized EMU is excellent with the speed of 160 km/h. However, due to the sustained swaying of the train tail in the single-track tunnel, the ride comfort of the tail carbody is poor, which drawn the attention of the railway department. Many field tests have been carried out by researchers to analyze the vibration characteristics of trains during operation. Zhai et al. [42] conducted the on-track field test on the CRH2C high-speed EMU to evaluate the dynamic performance of the train. Wang et al. [43] tracked the CRH380B series high-speed trains to monitor the evolution of vehicle dynamic behavior with wheel wear process. Shi et al. [44] carried out the experimental study on 300 km/h high-speed trains, and introduced the methods to analyze the train stability, ride quality and wheel wear evolution.

5.1 Test conditions

The test line was the Yuxi-Mengzi railway in Yunnan, China, with the characteristics of large proportion of tunnel lines. The railway line from Yuxi to Mengzi was officially opened in 2019, with a total length of 150 km. Among them, there are 35 tunnels and 61 bridges, accounting for 55%

of the total length of the line. Then, in November 2022, our research group carried out the on-track test on the typical short marshalling train of the Power Centralized EMU, as shown in Figure 8(a), which consists of eight vehicles (one powered vehicle + seven trail vehicles). The dynamic performance of the powered vehicle at the train tail was tested and analyzed.

(a)

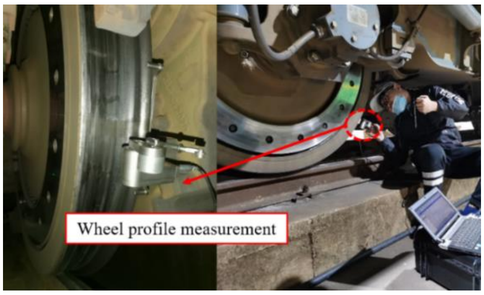

(b)

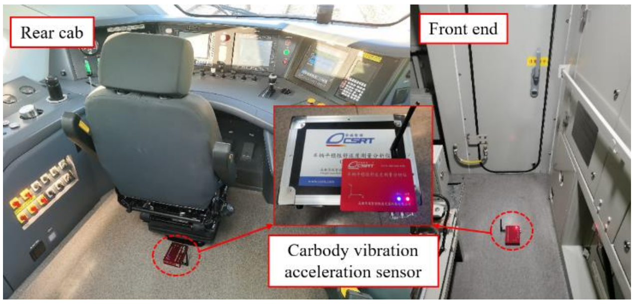

(c)

Figure 8. Test conditions: (a) the tested Power Centralized EMU;

(b) measurement of wheel profiles; (c) measurement of carbody's vibration.

Wheel-rail contact state is important for railway vehicle dynamics, which affects the ride comfort and stability of railway vehicles [1]. Therefore, the two typical wheel profiles of the rear powered vehicle were measured as shown in Figure 8(b), including JM3 new wheel profile after wheel re-profiling and the worn wheel profile after running 69,000 km. Additionally, two carbody vibration acceleration sensors are respectively installed on the surface of the carbody floor. As shown in Figure8(c), one is installed in the cab at the rear end of the powered vehicle and the other is installed in the equipment room at the front end of the powered vehicle. In order to accurately analyze the ride comfort of the vehicle, the sampling frequency of the acceleration sensor is set to 1000 Hz, and the range is 2 g (g is the gravitational acceleration, and the value is 9.8 m/s^2).

5.2 Wheel profiles measurement

As shown in Figure 9, the main wear region on the wheel tread concentrates on the adjacent area ranging from -20 to 30 mm around the nominal rolling circle. The max wear depth of the worn wheel is 0.58 mm after running 69,000 km, while the thickness of the flange remains unchanged. Then, the matching equivalent conicity λ at the wheel-rail contact lateral displacement 3 mm under the standard UIC60 rail was calculated. The equivalent conicity λ is about 0.10 under the JM3 new wheel profile, while the equivalent conicity λ increased to about 0.40 under the JM3 worn wheel profile.

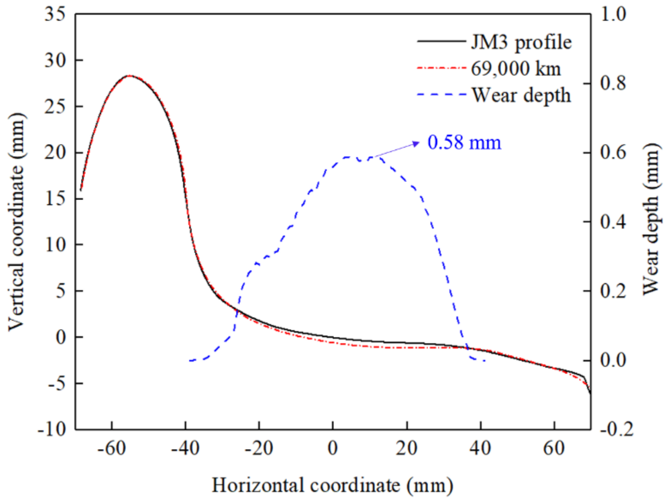

Figure 9. Wheel profile and wear depth of wheel tread.

5.3 Vibration acceleration of carbody

5.3.1 Open-line condition

As shown in Figure 10, the value of lateral ride comfort index W_y under the new or worn wheel is all below 2.75 with the train speed around 130 km/h, indicating that the lateral ride comfort is indeed excellent in open-line operation. Meanwhile, it can be seen from Figure 10(a) that under the new wheel, the lateral ride comfort of the rear cab is significantly worse than that of the front end.

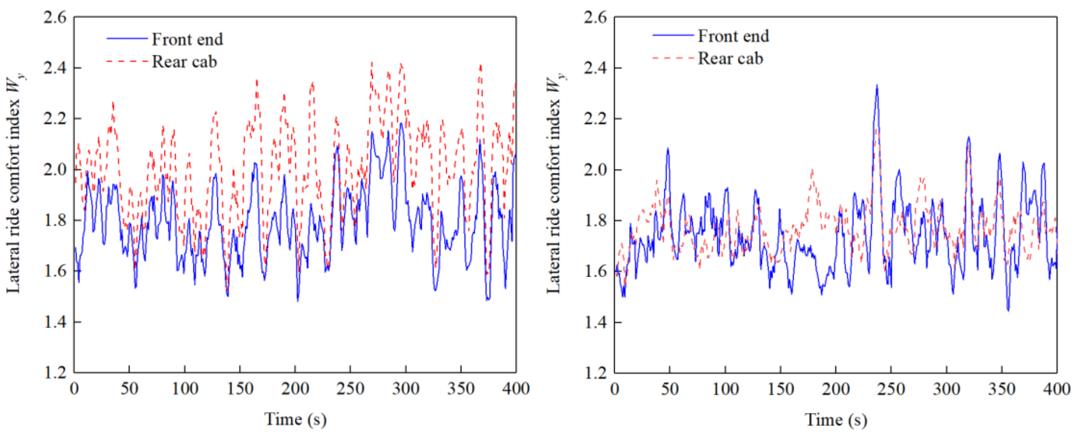

(a) (b)

Figure 10. Test results of carbody lateral ride comfort index W_y: (a) new wheel; (b) worn wheel.

Figure 11 shows the lateral vibration acceleration of the carbody's rear cab under the new and worn wheel in time and frequency domains, respectively. As shown in Figure 11(a,c), the peak value of the rear cab lateral acceleration under either new or worn wheels is usually within 0.05 g. Furthermore, as shown from Figure 11(b,d) that the lateral vibration dominant frequency of the rear cab under the new or worn wheel is all close to 1.3 Hz, which represents the vehicle hunting frequency at the speed of 130 km/h.

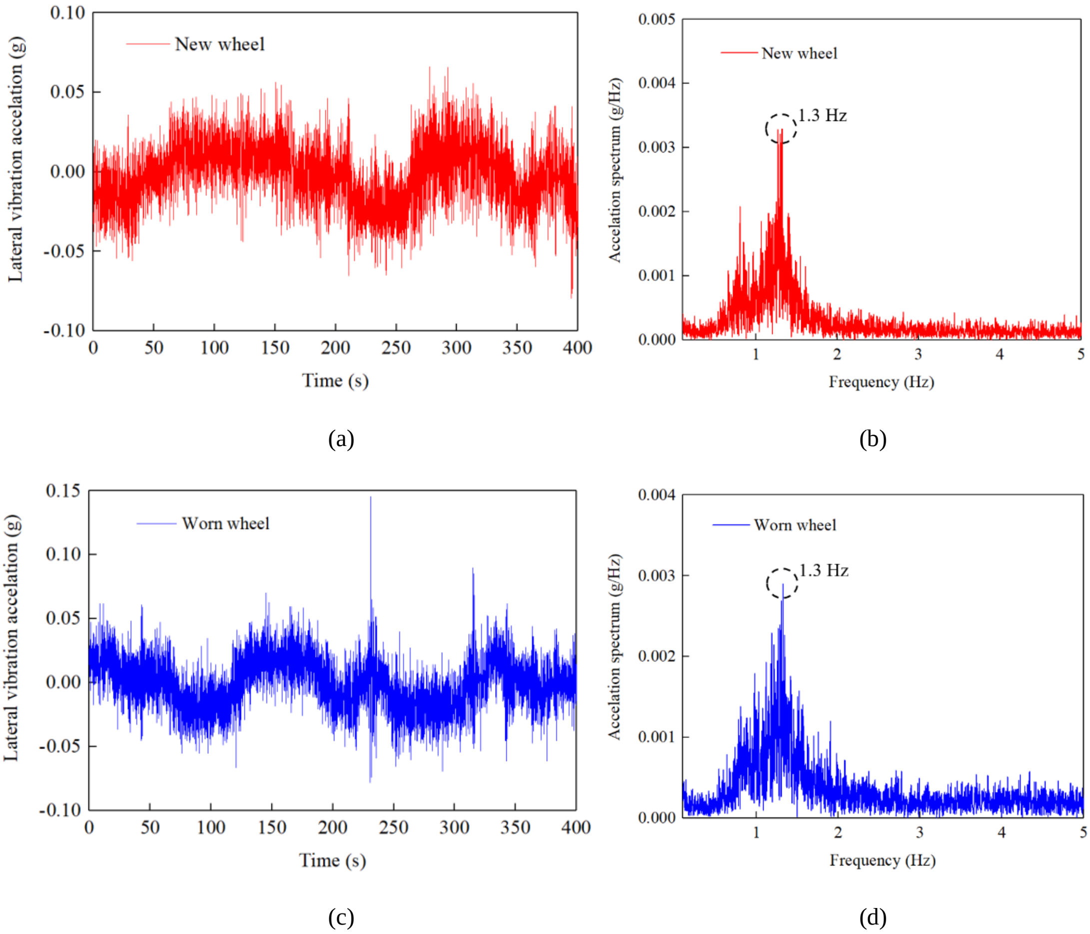

Figure 11. Test results of the rear cab lateral acceleration:

(a) time domain under new wheel; (b) frequency domain under new wheel;

(c) time domain under worn wheel; (d) frequency domain under worn wheel.

5.3.2 In-tunnel condition

The typical tunnel conditions are shown in Figure 12, which consist of two tunnels and a connecting bridge. Generally, the GPS module is used to measure the train speed. Due to the poor signal in the tunnel, we roughly recorded the operating speed of the train according to the driver's tachograph.

The running speed of the curved tunnel is around 117 km/h, the running speed in speed-limiting section of straight tunnel is around 60 km/h, and the running speed in other single-track straight tunnels is 120–130 km/h.

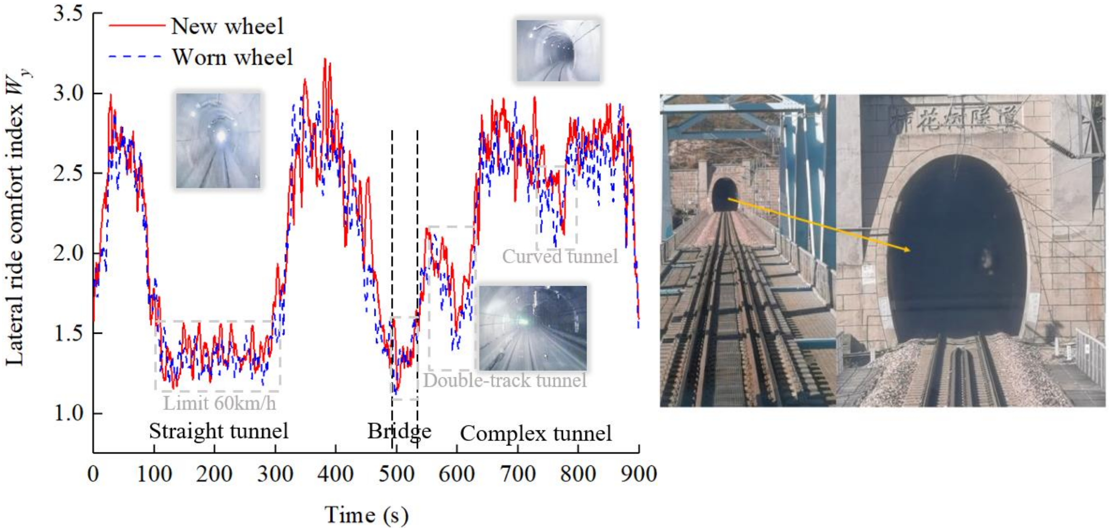

(a) (b)

Figure 12. Test results of tunnel operation:

(a) lateral ride comfort index W_y; (b) on-site photo of the tunnel.

The lateral ride comfort index W_y of the rear cab in tunnel operation is shown in Figure 12(a), of which the unmarked sections are single-track straight tunnels. It can be seen that during the operation of curved tunnel, the lateral ride comfort is good, because the wheel flange and rail are close together at this time, and the vibration of carbody is not violent. When operating in the double-track tunnel and speed-limiting straight tunnel, the aerodynamic effect is not obvious, and the lateral ride comfort is excellent. However, under the operation of single-track straight tunnel, when the speed increases to 120–130 km/h, the value of W_y is immediately increased to above 2.75, and the lateral ride comfort will deteriorate rapidly. Furthermore, the lateral ride comfort under JM3 new wheel is much better than that under worn wheel, as shown in Figure 12(a), and the peak values of the rear cab lateral ride comfort index W_y under new and worn wheel are 3.2 and 3.0, respectively.

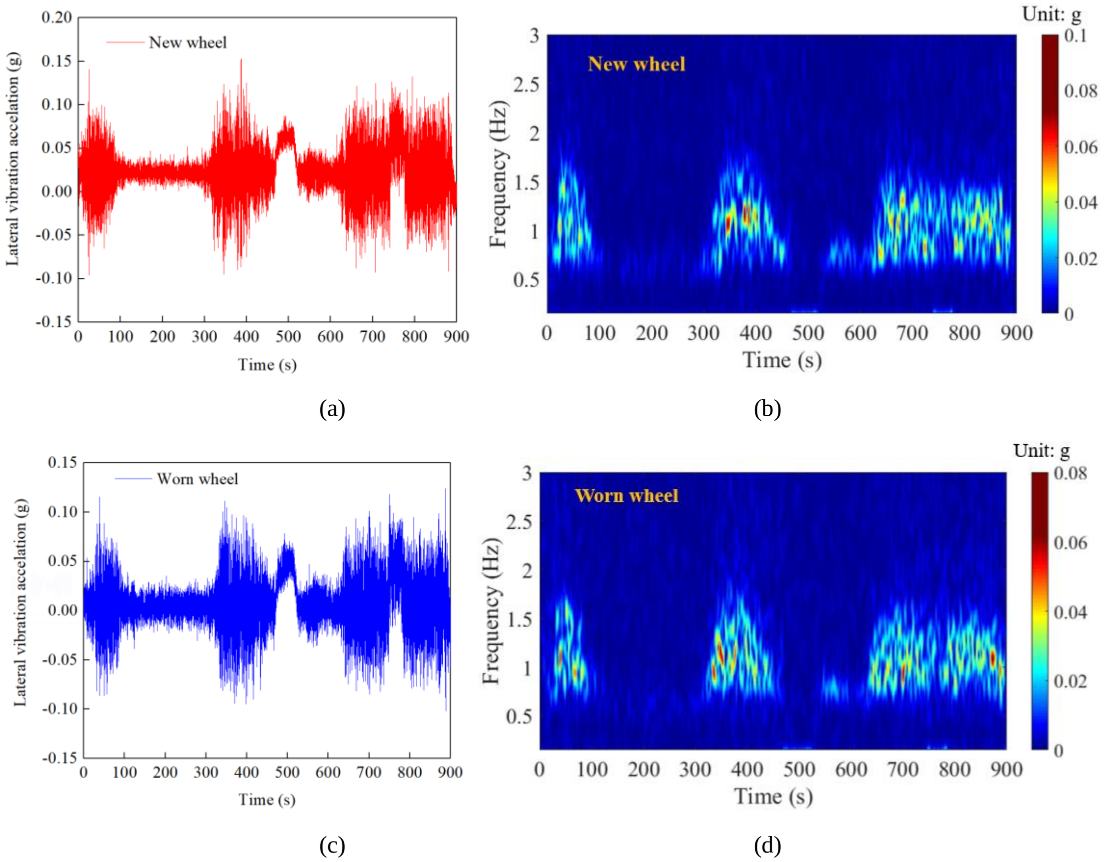

Figure 13. Test results of carbody lateral acceleration with tunnel operation:

(a) frequency domain under new wheel; (b) time-frequency under new wheel;

(c) frequency domain under worn wheel; (d) time-frequency under worn wheel.

The lateral vibration acceleration of the rear cab in tunnel operation is analyzed in Figure 13. As shown in Figure 13(a,c), when operating in the single-track straight tunnel, the lateral vibration acceleration of carbody under the new wheel is significantly higher than that under worn wheel. The lateral acceleration amplitude of the carbody reaches 0.15 g under new wheel, while the amplitude is 0.12 g under worn wheel. The corresponding time-frequency results are shown in Figure 13(b,d), it can be seen that the vibration energy of rear cab is mainly distributed in the range of 1–1.5 Hz due to the change of train operating speed in different track sections. Furthermore, under the condition of single-track tunnel with the worst ride comfort around 380 s, the train tail swaying frequency is dominated by 1.3 Hz of the vehicle hunting frequency.

In summary, the Power Centralized EMU performs well in terms of ride comfort on the open line, but the lateral ride comfort of the train tail is significantly decreased under single-track tunnel condition, which is caused by the aerodynamic effect of the wake vortex. However, is the lateral vibration of the train tail carbody related to the forced vibration induced by vortex shedding in the wake? If so, what is the vortex shedding frequency? According to the simulation and test results, the vortex shedding frequency is 1.7 Hz at the speed of 130 km/h, which is close to 1.3 Hz of the vehicle hunting frequency, thus vortex-induced vibration happens. With the increase of carbody swaying, the fluid-structure coupling effect will be enhanced. The fluid-structure coupling effect changes the vortex shedding frequency and causes structural resonance, which further deteriorates the ride comfort of the carbody. The swaying of the carbody is dominated by the vehicle hunting frequency.

6 Conclusion

Aiming at the swaying phenomenon of the rear powered vehicle of the Power Centralized EMU in single-track tunnels, the coupling simulation of aerodynamics and vehicle system dynamics, as well as on-track tests have been carried out, in which the various wheel-rail contact geometrical conditions are considered. The conclusions can be concluded:

(1) The simulation reappears the train tail sustained swaying phenomenon of the rear powered vehicle in single-track tunnels, indicating that the aerodynamic effect acting on the tail carbody is the main causing factor. The influence caused by wheel-rail contact geometry is consistent with the on-track test. The dominant frequency of sustained swaying is the same as the vehicle hunting frequency, and the vibration will be more violent under the condition of low equivalent conicity in wheel-rail contact.

(2) In the independent fluid simulation, the vortex shedding frequency of the train wake is 1.7 Hz at the speed of 130 km/h, which means the frequency of aerodynamic loads and the lateral vibration acceleration of carbody is 1.7 Hz. However, the dominant frequency of the carbody swaying is the vehicle hunting frequency of 1.3 Hz, which is identified in the on-track test and fluid-structure coupling simulation. This indicates that vortex-induced vibration (VIV) causes the frequency locking phenomenon. The fluid-structure coupling effect changes the vortex shedding frequency and causes structural resonance, therefore, the problem about train tail sustained swaying requires the fluid-structure coupling analysis.

(3) Based on the perspective of this study, reducing the fluid-structure coupling effect is

beneficial to weaken the sustained swaying phenomenon of the train tail in single-track tunnels. For instance, improving the primary hunting (i.e. carbody hunting) stability, as well as reducing the vibration amplitude of the carbody's rear-end through the improvement of suspension parameters are effective measures. Those measures have been confirmed in practice.

Disclosure statement

No potential conflict of interest was reported by the author(s).

Funding

The material in this paper is based on work supported by National Natural Science Foundation grant of China (U2268211), Sichuan Natural Science Foundation grant (2022NSFSC0034, 2022NSFSC1901), and Traction Power State Key Laboratory grant (2022TPL-T02) of the Independent Research and Development Projects.

References

[1] Li W, Guan QH, Chi MR, et al. An investigation into the influence of wheel-rail contact relationships on the carbody hunting stability of an electric locomotive. Proc IMechE Part F: J Rai Rapid Transit. 2022; 236(10):1198–1209.

[2] Shi YX, Dai HY, Wang QS, et al. Research on low-frequency swaying mechanism of metro vehicles based on wheel-rail relationship. Shock Vib. 2020; 2020(12):1–15.

[3] Sun JF, Chi MR, Jin XS, et al. Experimental and numerical study on carbody hunting of electric locomotive induced by low wheel-rail contact conicity. Veh Syst Dyn. 2021; 59:203–223.

[4] Li G, Yao Y, Shen LJ, et al. The influence of yaw damper layouts on locomotive lateral dynamics performance: Pareto optimization and parameter analysis. J Zhejiang Univ A. 2023; 24(5):450−464.

[5] Yao Y, Xu G, Song YD, et al. Mechanism of train tail lateral sway of EMUs in tunnel based on vortex-induced vibration. J Traffic Transp Eng. 2021; 21(5):51–61. [in Chinese].

[6] Liu DJ, Li XZ, Mei FL, et al. Effect of vertical vortex-induced vibration of bridge on railway vehicle's running performance. Veh Syst Dyn. 2022; 61(5):1432–1447.

[7] Zhou L, Ge YJ. Wind tunnel test for vortex-induced vibration of vehicle-bridge system section

model. J Braz Soc Mech Sci Eng. 2008; 30(2):110–117.

[8] Khier W, Breuer M, Durst F. Flow structure around trains under side wind conditions: a numerical study. Comput Fluids. 2000; 29(2):179–195.

[9] Hemida H, Krajnovic S. Exploring flow structures around a simplified ICE2 train subjected to a 30 degrees side wind using LES. Eng Appl Comp Fluid Mech. 2009; 3(1):28–41.

[10] Zhu TC, Li W. Numerical study of the trailing vehicle length on train aerodynamics under crosswind. AIP Adv. 2023; 13(2),025366.

[11] Huo XS, Liu TH, Yu M, et al. Impact of the trailing edge shape of a downstream dummy vehicle on train aerodynamics subjected to crosswind. Proc IMechE Part F: J Rai Rapid Transit. 2020; 235(2):201–214.

[12] Khayrullina A, Blocken B, Janssen W, et al. CFD simulation of train aerodynamics: Train-induced wind conditions at an underground railroad passenger platform. J Wind Eng Ind Aerodyn. 2015; 139:100–110.

[13] Choi JK, Kim KH. Effects of nose shape and tunnel cross-sectional area on aerodynamic drag of train traveling in tunnels. Tunn Undergr Space Technol. 2014; 41:62–73.

[14] Niu JQ, Zhou D, Liang XF, et al. Numerical simulation of the Reynolds number effect on the aerodynamic pressure in tunnels. J Wind Eng Ind Aerodyn. 2018; 173:187–198.

[15] Du JM, Fang Q, Wang G, et al. Aerodynamic effects produced by a high-speed train traveling through a tunnel considering different car numbers. Symmetry-Basel. 2022; 14(3),479.

[16] Fujimoto H, Miyamoto M, Shimamoto Y. Lateral vibration and its decreasing measure in the tail car of a Shinkansen. Trans Jpn Soc Mech Eng. 1993; 59(560):1016–1022.

[17] Takai H. Maintenance of track with long-wave track irregularity on Shinkansen. QR of RTRI. 1990; 3:13–20.

[18] Suzuki M. Unsteady aerodynamic force acting on high speed trains in tunnel. QR of RTRI. 2001; 42(2):89–93.

[19] Suzuki M. Flow-induced vibration of high-speed trains in tunnels. Lect Notes Appl Comput Mesh. 2004; 19:443–452.

[20] Diedrichs B, Berg M, Stichel S, et al. Vehicle dynamics of a high-speed passenger car due to aerodynamics inside tunnels. Proc IMechE Part F: J Rai Rapid Transit. 2007; 221(4):527–545.

[21] Diedrichs B, Krajnović S, Berg M. On the aerodynamics of car body vibrations of high-speed trains cruising inside tunnels. Eng Appl Comp Fluid Mech. 2008; 2(1):51–57.

[22] Tanifuji K, Sakanoue K, Kikko S. Modelling of aerodynamic force acting on high speed train in tunnel and a measure to improve the riding comfort utilising restriction between cars. Veh Syst Dyn. 2008; 46(S1):1065–1075.

[23] Kikko S, Tanifuji K, Sakanoue K, et al. Modeling of aerodynamic force acting in tunnel for analysis of riding comfort in a train. J Mech Sys Trans Logist. 2008; 1(1):31–42.

[24] McNamara G, Zanetti G. Using the Boltzmann equation to simulate lattice-gas automata. Phys Rev Lett. 1988; 61:2332–2335.

[25] Chen S, Doolen GD. Lattice boltzmann method for fluid flows. Annu Rev Fluid Mech. 2003; 30(1):329–364.

[26] Sbragaglia M, Benzi R, Biferale L, et al. Generalized lattice boltzmann method with multirange pseudopotential. Phys Rev E. 2007; 75(2),026702.

[27] Xu AG, Zhang GC, Gan YB, et al. Lattice Boltzmann modeling and simulation of compressible flows. Front Phys. 2012; 7(5):582–600.

[28] SIMULIA, Inc., SIMULIA Xflow User's Guide, Release 2021x.

[29] Hemida H, Krajnovi S. LES study of the influence of the nose shape and yaw angles on flow structures around trains. J Wind Eng Ind Aerodyn. 2010; 98(1):34−46.

[30] Nakade K. Numerical simulation of flow around railway vehicle in turbulent boundary layer over flat terrain. QR of RTRI. 2014; 55(4):249–253.

[31] Osth J, Krajnovic S. A study of the aerodynamics of a generic container freight wagon using Large-Eddy Simulation. J Fluids Struct. 2014; 44:31–51.

[32] Niu JQ, Liang XF, Zhou D. Experimental study on the effect of Reynolds number on aerodynamic performance of high-speed train with and without yaw angle. J Wind Eng Ind Aerodyn. 2016; 157:36–46.

[33] GB 146.2-2020 Gauge for standard gauge railways Part 2: Structure gauge. [in Chinese].

[34] Li L, Liu TH, Guo ZJ, et al. On the effect of rail-end slope in train aerodynamics under crosswind. Veh Syst Dyn. 2021; 60(6):1888−1908.

[35] BS EN, Railway Applications–Aerodynamics Part 6: Requirements and Test Procedures for

Crosswind Assessment (British Standard Institute, London, 2018), no. 14067–6.

[36] Iwnicki S. Simulation of wheel–rail contact forces. Fatigue Fract Eng Mater Struct. 2003; 26:887–900.

[37] Li JY, Liu LY, Kou DH. Wu Guang high-speed rail track irregularity power spectrum analysis. Appl Mech Mater. 2014; 638–640:1224–1228.

[38] Li G, Wu RD, Deng XX, et al. Suspension parameters matching of high-speed locomotive based on stability/comfort Pareto optimization. Veh Syst Dyn. 2022; 60(11):3848−3867.

[39] Li G, Zhou Y, Yuan Yao, et al. Application of yaw dampers with frequency-selective damping to improve the locomotive adaptability to low/high conicity stability. Proc IMechE Part F: J Rai Rapid Transit. 2022. DOI: 10.1177/09544097221141517.

[40] Peng Y, Zhou JH, Fan C, et al. A review of passenger ride comfort in railway: assessment and improvement method. Transp Saf Environ. 2022; 4(2),17.

[41] National Railway Administration, 2019. GB/T5599. Specification for dynamics performance assessment and testing verification of rolling stock. Beijing, China. [in Chinese].

[42] Zhai WM, Liu PF, Lin JH, et al. Experimental investigation on vibration behaviour of a CRH train at speed of 350 km/h. Int J Rail Transp. 2015; 3(1): 1–16.

[43] Wang JB, Song CY, Wu PB, et al. Wheel reprofiling interval optimization based on dynamic behavior evolution for high-speed trains. Wear. 2016; 366(S1):316–324.

[44] Shi HL, Wang JB, Wu PB, et al. Field measurements of the evolution of wheel wear and vehicle dynamics for high-speed trains. Veh Syst Dyn. 2018; 56(8):1187–1206.

Dear Editors,

This is a manuscript of a full paper by Yadong Song, Ting Qin, Yuan Yao, and Fengyu Dai titled "Investigation on aerodynamic fluid-structure coupling vibration of 160 km/h EMU tail in single-track tunnels". It is submitted to be considered for publication in your journal. Neither the entire paper nor any part of its content has been published or accepted elsewhere. It is not being submitted to any other journal.

Since the operation of the Power Centralized EMU (Electric Multiple Unit) with a speed of 160 km/h in 2019, the EMUs have appeared different lateral dynamics problems. Recently, the phenomenon about tail sustained swaying of the 160 km/h EMU in single-track tunnels has gained much attention, especially for the rear powered vehicle. This phenomenon is investigated from the perspective of aerodynamic fluid-structure coupling vibration in this study. For the first time, the vortex-induced vibration (VIV) is proposed in the fluid-structure coupling of the train tail.

The aerodynamics simulation model of the train in tunnels and the multi-body dynamics model of the rear powered vehicle were respectively established through the software of XFlow and Simpack, and then the fluid-structure coupling vibration was simulated using real-time data dynamic exchange between the two models. Moreover, the carbody's vibration acceleration and the aerodynamic load acting on the carbody under various wheel-rail contact geometrical conditions were discussed. Finally, the train tail swaying in field was tested, and the dominant frequencies were analyzed. The results show that the periodic aerodynamic loads and the frequency locking effect caused by the coupled vibration are the main factors for the ride comfort deterioration.

For the vehicle in this work, according to the simulation and test results, the vortex shedding frequency is 1.7 Hz at the speed of 130 km/h, which is close to 1.3 Hz of the vehicle hunting frequency, thus vortex-induced vibration happens. With the decrease of equivalent conicity in wheel-rail contact, the amplitude of carbody swaying increases owing to the carbody hunting, the fluid-structure coupling effect will be enhanced. The fluid-structure coupling effect changes the vortex shedding frequency and causes structural resonance, which further deteriorates the ride comfort of the carbody. The swaying of the carbody is dominated by the vehicle hunting frequency, and the improvement of vehicle lateral stability can weaken this phenomenon.

We believe this paper may be of particular interest to the readers of your journal.

Correspondence and phone calls about the paper should be directed to Yuan Yao at the following address, phone and fax number, and e-mail address:

State Key Laboratory of Traction Power,

Southwest Jiaotong University,

Chengdu 610031, China

Tel: 86-28-86466209

Fax: 86-28-87600868

E-mail: yyuan8848@163.com

Thanks very much for your attention to our paper.

Sincerely yours,

Yuan Yao

Author Agreement

Click here to access/download;Author Agreement;Author_agreement.jpg

WORLD SCIENTIFIC PUBLISHING COMPANY PTE LTD
5 Toh Tuck Link, Singapore 596224
Fax: (65) 6467 7667

Copyright Transfer Form

To the extent transferable, copyright in and to the undersigned Author's article ("Article") entitled

《Investigation on aerodynamic fluid-structure coupling vibration of 160 km/h EMU tail in single-track tunnels》

Title

By

[illegible] [illegible] [illegible] 代凤羽

Authors

is hereby assigned to World Scientific Publishing Company Pte Ltd. for publication.

The article will be published in the

International Journal of Structural Stability and Dynamics

The Author represents that he is the author and proprietor of this Article, that he has full power to make this Agreement on behalf of himself and his co-authors, and that this Article has not heretofore been published in book form. The Author shall obtain written permission and pay all fees for use of any literary or illustration material for which rights are held by others. The Author agrees to hold the Publisher harmless against any suit, demand, claim or recovery, finally sustained, by reason of any violation of proprietary right or copyright, or any unlawful matter contained in this Article.

Signature

[illegible]

Name of Author

Southwest Jiaotong University. China

Institution or Company

2023.8.14

Date